

DeepH-2: Enhancing deep-learning electronic structure via an equivariant local-coordinate transformer

Yuxiang Wang,^{1,*} He Li,^{1,2,*} Zechen Tang,^{1,*} Honggeng Tao,¹ Yanzhen Wang,¹ Zilong Yuan,¹ Zezhou Chen,¹ Wenhui Duan,^{1,2,3,†} and Yong Xu^{1,3,4,‡}

¹*State Key Laboratory of Low Dimensional Quantum Physics and Department of Physics, Tsinghua University, Beijing, 100084, China*

²*Institute for Advanced Study, Tsinghua University, Beijing 100084, China*

³*Frontier Science Center for Quantum Information, Beijing, China*

⁴*RIKEN Center for Emergent Matter Science (CEMS), Wako, Saitama 351-0198, Japan*

Deep-learning electronic structure calculations show great potential for revolutionizing the landscape of computational materials research. However, current neural-network architectures are not deemed suitable for widespread general-purpose application. Here we introduce a framework of equivariant local-coordinate transformer, designed to enhance the deep-learning density functional theory Hamiltonian referred to as DeepH-2. Unlike previous models such as DeepH and DeepH-E3, DeepH-2 seamlessly integrates the simplicity of local-coordinate transformations and the mathematical elegance of equivariant neural networks, effectively overcoming their respective disadvantages. Based on our comprehensive experiments, DeepH-2 demonstrates superiority over its predecessors in both efficiency and accuracy, showcasing state-of-the-art performance. This advancement opens up opportunities for exploring universal neural network models or even large materials models.

I. INTRODUCTION

Ab initio calculations based on density functional theory (DFT) have become pivotal in the realm of computational materials discovery. Their low computational efficiency, however, poses a critical constraint on various applications, such as the investigation of large-size materials and the building of big materials databases. To surmount this challenge, the integration of artificial intelligence (AI) emerges as a promising avenue. The central idea is to model the intricate input-output relationship of DFT by neural networks. By leveraging knowledge acquired from DFT training calculations on small materials structures, the aim is to empower the neural networks to generalize effectively, enabling predictions for previously unseen, large materials structures. To date, the transferability from small to large scales has been demonstrated in two fundamental models of DFT. These include the atomic-structure model, which utilizes deep-learning force fields [1–9], and the electronic-structure model employing deep-learning DFT Hamiltonian (DeepH) [10–15]. This success is attributed to the adherence to the nearsightedness principle by these models [16]. The notable transferability presents opportunities for the exploration of large materials models, akin to the well-established large language models. While the current research within the field predominantly focuses on the atomic-structure model, a comprehensive understanding of the intriguing quantum effects in materials necessitates a more profound exploration at the electronic structure level.

Several neural-network architectures have been devised for deep-learning electronic structure. In these architectures, it is imperative that the relationship between input materials structures and output DFT electronic structures maintains equivariance to the Euclidean group in three-dimensional (3D) space, denoted as the $E(3)$ group. The symmetry requirement represents a fundamental prior knowledge that can substantially improve data efficiency and enhance generalization capability. In the original model of DeepH, the equivariance is preserved by combining $E(3)$ -invariant networks with local-coordinate transformations. While local-coordinate neural networks (LCNNs) are relatively straightforward to implement, their accuracy is constrained by the lack of a proper strategy for selecting appropriate local coordinates [10]. In the DeepH-E3 framework, more stringent requirements are imposed: all input, internal, and output feature vectors must respect $E(3)$ -equivariance, and their interactions must follow the principle of group theory. This not only limits the expressive power and but also significantly increases the computational workload [11]. For instance, as the number of angular momentum channels increases, the computational cost of ENNs grows with $O(L^6)$, where L denotes the highest angular momentum quantum number. Recent studies in deep-learning force fields have successfully decreased the computational cost to $O(L^3)$ by integrating local coordinates into ENNs, resulting in enhanced model performance [17, 18]. Extending this approach to deep-learning electronic structure holds great promise, considering the prevalence of high- L channels in this field of study. The corresponding research, however, is currently missing.

In this work, we introduce DeepH-2, a neural-network approach aimed at enhancing deep-learning electronic structure. DeepH-2 incorporates ENNs, local-coordinate transformations, and transformer models into a unified framework called the equivariant local-coordinate trans-

* These authors contributed equally to this work.

† duanw@tsinghua.edu.cn

‡ yongxu@mail.tsinghua.edu.cn

former (ELCT). In DeepH-2, instead of choosing the full local coordinate system as DeepH, only a local-coordinate z -axis is selected for each edge and aligned naturally along the edge direction. By this local-coordinate transformation, the non-Abelian $SO(3)$ group of traditional ENNs is reduced to the Abelian $SO(2)$ group. Thus channels of different angular momenta in ELCT can be directly mixed and become suitable for GPU parallel computing. Moreover, ELCT adopts the classical architecture of transformer models, empowering the networks to employ multi-head attention for extracting diverse features. This enables a more comprehensive description of the relationship between material structures and electronic structures. All these enhancements significantly boost the expressive power and computational efficiency of DeepH-2, resulting in substantially improved performance compared to preceding models like DeepH and DeepH-E3.

II. PHYSICS PRIOR KNOWLEDGE

In DFT, a key quantity of electronic structure calculations is the DFT Hamiltonian, from which all the physical properties in the single-particle picture can be derived [19]. The neural network representation of DFT Hamiltonians is guided by two fundamental physical principles, including the nearsightedness principle of electronic matter [16, 20] and the principle of covariance. To ensure compatibility with these principles, DFT Hamiltonians under numerical atomic bases (NAO) are selected as the target for deep learning. The NAO takes the form $\phi_{ipml}(\mathbf{r}) = R_{ipl}(r)Y_{lm}(\hat{r})$, representing an orbital centered on atom i with multiplicity index p and angular dependence described by a spherical harmonics Y_{lm} of degree l and order m . The Hamiltonian matrix is therefore denoted as $[H_{ij}]_{l_1 l_2; m_1 m_2}^{p_1 p_2}$. H_{ij} is the Hamiltonian matrix block between atoms i and j , which vanishes for distance atom pairs due to the confined nature of the radial function $R_{ipl}(r)$. In the context of designing the neural network, the nearsightedness principle is typically treated with message-passing neural network based on crystal graphs. Each atom corresponds to a vertex (or node) of the graph, and only atom pairs within a distance R_C are considered. The nearsightedness principle is reflected by a finite R_C and a finite number of message passing layers. This graph neural network architecture enables the $O(N)$ scaling of the network, facilitating the study of large-scale materials systems.

Incorporating symmetry knowledge, however, requires careful design of neural network. Formally, the neural network must establish a mapping f_{NN} from the materials structure $\{\mathcal{R}\}$ to the DFT Hamiltonian matrix elements $[H_{ij}]_{l_1 l_2; m_1 m_2}^{p_1 p_2}$. This mapping should exhibit equivariance to the $E(3)$ group by satisfying $D_H(g) \circ f_{\text{NN}} = f_{\text{NN}} \circ D_{\{\mathcal{R}\}}(g)$ for arbitrary $g \in E(3)$, where $D_{\{\mathcal{R}\}}$ and D_H are representations of the $E(3)$ group on materials structures and Hamiltonian, respectively. While the

translation equivariance is naturally maintained by taking only relative atomic positions into concern, the rotational equivariance could bring up non-trivial issues regarding the complex transformation of Hamiltonian matrix elements. Given the difficulty and inefficiency in learning the equivariant relations via data augmentation, the former implementation of deep-learning electronic structure all integrated the equivariance feature directly into the design of neural networks. An overview of the methods employed to implement the rotational equivariance is summarized in Fig. 1.

The initial version of DeepH addressed the rotation equivariant feature by transforming it into an invariant one, employing a strategy based on local coordinates (Fig. 1). The Hamiltonian matrix block H_{ij} is mapped to a deterministic local coordinate, defined by the positions of atoms i and j together with the nearest neighbor of atom i . Consequently, H_{ij} in local coordinates remain invariant under global structural rotations. This enables a flexible learning through an invariant neural network, resulting in accuracy at the meV level across multiple case studies.

However, DeepH exhibits notable limitations stemming from the LCNN scheme. The determination of local coordinate relies on the position of the nearest neighbor of atom i , possibly rendering the neural network non-smooth with respect to structural changes. This discontinuity poses challenge to DeepH's applications in molecular dynamics simulations. Consequently, the generalizability of DeepH is affected by the abrupt choice of local coordinate, as the discontinuity when changing local coordinates necessitates an enormous amount of training data, thereby limiting DeepH's performances.

Concerning the limitations of DeepH, a subsequent development, DeepH-E3 utilizes the lately developed architecture named ENNs [21] to guarantee the $E(3)$ equivariance across all the internal features of the neural networks, making full use of equivariant knowledge without introducing a local coordinate (Fig. 1). In essence, all neural network features comprise a direct sum of equivariant vectors labelled by the angular momentum $l = 0, 1, 2, \dots$. An equivariant vector $\mathbf{x}^l = (x_{l,l}, x_{l,l-1}, \dots, x_{l,-l})$ possesses a dimension of $2l+1$, and undergoes a transformation $\mathbf{x}^l = \mathbf{D}^l(\mathbf{R})\mathbf{x}^l$ upon spatial rotation \mathbf{R} , where $\mathbf{D}^l(\mathbf{R})$ represents the Wigner-D matrix. Structural information enters the neural networks as equivariant vectors through embedding with scalar functions or spherical harmonic functions. Neural network operations are carefully restricted to preserve the equivariance of internal features. Hamiltonian matrix blocks can be divided into equivariant tensors $l_1 \otimes l_2$, and expressed in terms of equivariant vectors utilizing the Wigner-Eckart theorem. The framework of ENNs is also extended to deal with spin-orbit coupling and to study magnetic materials [11, 12].

Leveraging the principle of equivariance, DeepH-E3 can outperform DeepH in case studies, achieving sub-meV prediction accuracy. However, it has been

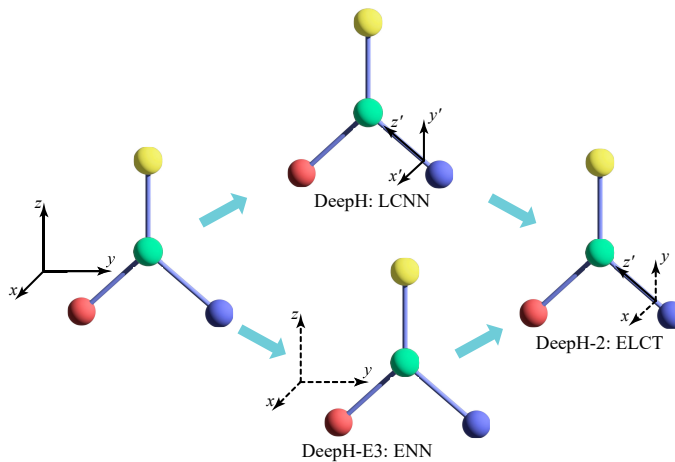


FIG. 1. Development path of DeepH-2. Two approaches for achieving equivariance in predicting the DFT Hamiltonians from materials structures have been established. A method based on local-coordinate transformations, named the local-coordinate neural network (LCNN) was proposed by the original work of DeepH [10]. Another method based on the equivariant neural network (ENN) was developed by DeepH-E3 [11]. DeepH-2 uses a new method utilizing the equivariant local-coordinate transformer (ELCT) that incorporates advantages of the two previous methods. The balls represent atoms, and the sticks connecting them represent bonds. Different kinds of coordinate systems are used here. The coordinates on the bonds indicate local coordinates, while those on the left-hand side of the four-atom structure indicate global coordinates. Solid axes imply specific choices of axes, and dashed ones signify that their particular selections are arbitrary.

observed that the neural network operations are significantly constrained due to the equivariant requirement within the DeepH-E3 framework. Coupling between features with different l is limited to the tensor product layers, defined by the equation: $z_{cm}^l = \sum_{l_1 l_2} \sum_{m_1 m_2} \sum_{c_1 c_2} C_{l_1 m_1; l_2 m_2}^{l m} (U_{cc_1}^{l_1} x_{c_1 m_1}^{l_1}) (V_{cc_2}^{l_2} y_{c_2 m_2}^{l_2})$, abbreviated as $\mathbf{z} = (\mathbf{U}\mathbf{x}) \otimes (\mathbf{V}\mathbf{y})$, where \mathbf{x} , \mathbf{y} , \mathbf{z} are equivariant features with channel index c , \mathbf{U} , \mathbf{V} are learnable parameters, and $C_{l_1 m_1; l_2 m_2}^{l m}$ denotes Clebsh-Gordan coefficients. The tensor product operation yields an overall $O(L^6)$ complexity for computing all $z_{cm}^{(l)}$. This high scaling over the highest angular momentum L heavily bottlenecks the incorporation of higher-angular momentum features. Moreover, the tensor product operation is also challenging to express solely with tensor operations, leading to limited GPU performance. Redundancy in parameters is also evident in tensor products, leading to an inefficient utilization of parameters in $U_{cc_1}^{l_1}$ and $V_{cc_2}^{l_2}$.

Addressing the aforementioned limitations associated with tensor products, DeepH-2 (Fig. 1) adopts the ELCT scheme, in analogy to the equivariant spherical channel network that was recently proposed to perform high-performance tensor product by leveraging $SO(2)$ operations [17]. Within this framework, tensor product operations are conducted between equivariant features $x_{m_1}^{l_1}$ and spherical harmonic projections of relative atomic positions $Y_{l_2 m_2}(\mathbf{r}_{ij})$. From the equivariance requirement, any neural network operation f acting on \mathbf{x}^{l_1} must satisfy the relationship:

$$f(\mathbf{x}^{l_1}) = \mathbf{D}^{l_1}(\mathbf{R}^{-1}) \circ f(\mathbf{D}^{l_1}(\mathbf{R}) \circ \mathbf{x}^{l_1}), \quad (1)$$

where \mathbf{R} is an arbitrary spatial rotation. As for the ten-

sor product mentioned above, a local coordinate transformation \mathbf{R} can be selected to align the z -axis with the relative atomic position \hat{r}_{ij} . Consequently, $Y_{l_2 m_2}(\hat{r}_{ij})$ exhibits sparsity in the transformed coordinate system, in the sense that $Y_{l_2 m_2}(\hat{z})$ is non-zero only for $m_2 = 0$ components. The sparsity of Clebsh-Gordan coefficients is exploited, as $C_{l_1 m_1; l_2 m_2}^{l m}$ is non-zero only for $m_1 = \pm m$, given $m_2 = 0$. The reduction of computational scaling from $O(L^6)$ to $O(L^3)$ can be attributed to these sparsity properties. Under the local coordinate, the transformed equivariant vectors $\tilde{x}_{m_1}^{l_1} = \mathbf{D}^{l_1}(\mathbf{R}) \circ \mathbf{x}^{l_1}$ are mapped to carry reducible representations of $SO(2)$, in contrast to carrying irreducible representations of $SO(3)$ in the global coordinate. Specifically, only rotations around \hat{r}_{ij} are relevant for $\tilde{x}_{m_1}^{l_1}$, and the transformation rule writes:

$$\begin{pmatrix} \tilde{x}_{m_1}^{l_1} \\ \tilde{x}_{-m_1}^{l_1} \end{pmatrix} \rightarrow \begin{pmatrix} \cos(m_1 \theta) & -\sin(m_1 \theta) \\ \sin(m_1 \theta) & \cos(m_1 \theta) \end{pmatrix} \begin{pmatrix} \tilde{x}_{m_1}^{l_1} \\ \tilde{x}_{-m_1}^{l_1} \end{pmatrix}, \quad (2)$$

in which θ denotes the rotation angle around \hat{r}_{ij} . Noting vectors under local coordinate with the same m transforms in the same manner, this facilitates mixing between channels with different l . Recalling that message passing between features with different l is heavily constrained in the DeepH-E3 scheme, this newfound flexibility enhances the neural network's expressiveness while maintaining equivariance throughout the network.

In contrast to previous works on deep-learning force fields, DeepH-2 is specifically designed for predicting DFT Hamiltonian matrices. Analogous to the approach taken in DeepH-E3, we note that Hamiltonian blocks $[H_{ij}]_{l_1 l_2; m_1 m_2}^{p_1 p_2}$ can be divided into sub-blocks $\mathbf{h} \equiv [H_{ij}]_{l_1 l_2}^{p_1 p_2}$ with elements $\mathbf{h}_{m_1 m_2}$. Each sub-block has di-

mension $(2l_1 + 1) \times (2l_2 + 1)$ and represents an equivariant tensor carrying representation $l_1 \otimes l_2$. The Wigner-Eckart theorem is employed to express the equivariant tensor with equivariant feature vectors. In specific, we have:

$$l_1 \otimes l_2 = |l_1 - l_2| \oplus |l_1 - l_2 + 1| \oplus \dots \oplus (l_1 + l_2). \quad (3)$$

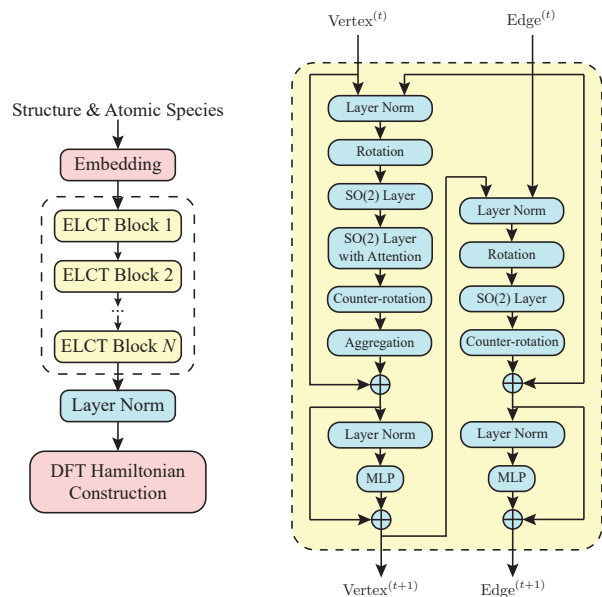
When the spin-orbit coupling is considered, the Hamiltonian matrix is also labelled with spin $\sigma_1, \sigma_2 \in \{\uparrow, \downarrow\}$. The Hamiltonian sub-blocks have elements $\mathbf{h}_{m_1 m_2}^{\sigma_1 \sigma_2}$, which will be represented by 4th-order equivariant tensors $(l_1 \otimes \frac{1}{2}) \otimes (l_2 \otimes \frac{1}{2})$. The high-order tensors can also be expressed in terms of equivariant vectors according to Eq. 3.

The advantage of DeepH-2 architecture over DeepH-E3 could be viewed from several perspectives. Incorporation of the ELCT scheme alleviates the heavy constraints on neural network operations imposed by equivariance, enhancing the expressiveness of DeepH-2. Moreover, ELCT takes full advantage of the sparsity of Clebsch-Gordan coefficients and significantly reduces the computational cost of tensor product, which is the most time-consuming part of ENNs. As a result, DeepH-2 can accommodate more learnable parameters compared to DeepH-E3. Intuitively, a DeepH-2 model with 10^7 learnable parameters exhibit comparable efficiency with a DeepH-E3 model with 10^6 parameters, enabling the training of more powerful neural network with similar computational resources. Given the large number of matrix elements to be predicted in the Hamiltonian, having a substantial number of parameters proves beneficial. Lastly, DeepH-2 incorporates a suite of advanced neural network techniques including equivariant transformer, such as EquiformerV2 [18], which are discussed in section III C. With all these benefits, it is also noteworthy that DeepH-2 is inherently an equivariant neural network, meaning all internal features are SO(3) equivariant, thereby preserving the exploitation of physical symmetry knowledge. Although local coordinates are specified in DeepH-2, only one axis of the coordinate is relevant. The determination of this axis is natural when studying atom pairs, thus eliminating any smoothness issues present in the original DeepH implementation.

III. ARCHITECTURE

A. Overview

An overview the network architecture is demonstrated in Fig. 2(a). The network takes structural information $\{\mathcal{R}\}$, including the atomic positions \mathbf{r}_i and the atom species index z_i as inputs and predicts the DFT Hamiltonian as the output. The neural network utilizes Graph Neural Network (GNN) framework, where each atom corresponds to a vertex \mathbf{v}_i and atom pairs are represented as edges \mathbf{e}_{ij} . Only atom pairs with distances less than



(a) Overall architecture (b) Structure of an ELCT block

FIG. 2. Network architecture of DeepH-2. (a) Schematic overview of the neural-network architecture. (b) Architecture of the equivariant local-coordinate transformer (ELCT) block. Message passing within DeepH-2 is achieved through connecting multiple ELCT blocks.

R_C are connected by edges, where R_C typically ranges from 6 to 10 Å, defined by two times the cutoff radius of the NAOs. Vertices connected with \mathbf{v}_i are defined as the neighborhood of vertex i , denoted \mathcal{N}_i . edge and vertex features are initiated via equivariant embedding of input data. Subsequently, network features are updated using several equivariant transformer blocks through message passing with nearby features. The output Hamiltonian matrix blocks are constructed from edge (vertex) features for off-site (on-site) blocks, respectively. The construction of Hamiltonian blocks are based on the Wigner-Eckart theorem displayed in Eq. 3.

B. Equivariant embedding

The embedding blocks aim to initiate equivariant features from structural information. In the context of embedding process, two types of information are relevant: the relative position of atom pairs r_{ij} and atom species index z_i . Benefiting from the relaxed equivariance constraint in the local-coordinate scheme, a more flexible equivariant embedding scheme is adopted. Under local-coordinates, all features with $m = 0$ remain invariant under spatial rotation, allowing for their embedding from scalar inputs such as $|r_{ij}|$ and z_i . This stands in contrast to the DeepH-E3 architecture, in which scalar inputs can only be embedded into features with $l = m = 0$. The embedding into edge features \mathbf{e}_{ij} is based on local-

coordinate determined by \hat{r}_{ij} , and the embedding involves $|r_{ij}|, z_i$ and z_j . Vertex features \mathbf{v}_i are embedded with z_i as well as $|r_{ij}|$ and z_j for all $j \in \mathcal{N}_i$. For each $j \in \mathcal{N}_i$, a local coordinate is established based on \hat{r}_{ij} , and embedding is performed with $|r_{ij}|, z_i$ and z_j . The embedding result from different j are then transformed back to the global coordinate and aggregated into \mathbf{v}_i . Noting the $m = 0$ constraint for feature embedding is only applicable under local coordinates, thereby no explicit constraint on components of embedded features is present.

C. ELCT blocks

Inspired by EquiformerV2 [18], DeepH-2 employs ELCT blocks featuring equivariant attention mechanism for message passing. In each ELCT block, every edge and vertex feature is updated using nearby features. The update of edge features \mathbf{e}_{ij} involves $\mathbf{v}_i, \mathbf{v}_j$ and \mathbf{e}_{ij} , computed under the local coordinate determined by \hat{r}_{ij} . Similarly, the update of vertex features \mathbf{v}_i incorporates \mathbf{e}_{ij} and \mathbf{v}_j for all $j \in \mathcal{N}_i$. For each j , an update procedure is performed with $\mathbf{v}_i, \mathbf{v}_j$ and \mathbf{e}_{ij} as input under the local coordinate determined by \hat{r}_{ij} , yielding an update component to \mathbf{v}_i , denoted \tilde{v}_i^j . Following the computation of all \tilde{v}_i^j , an attention block calculates an attention weight α_i^j for each atom j . Each \tilde{v}_i^j is then weighted by α_i^j and added to \mathbf{v}_i .

The design of ELCT blocks may be justified from two perspectives. Edge and vertex features are updated by nearby features, which corresponds to the message passing on the crystal graph. This design makes DeepH-2 compatible with the nearsightedness principle, and ensures its size extensiveness and scalability to large systems. An attention mechanism is introduced in vertex updates, assigning weights to the updates from all edges. Physically, the influence of edges (bonds) on vertices (atoms) may vary and has complicated dependencies on the atomic environment. Introducing attention helps discern these intricate dependencies. For predicting DFT Hamiltonians, the interactions between orbitals of high angular momenta will be considered. The use of ELCT blocks could substantially improve the treatment of high-angular-momentum channels, and the potential gain is much more significant compared to deep-learning force fields that typically involve lower-angular-momentum channels.

IV. RESULTS

We evaluated the accuracy and efficiency of DeepH-2 using monolayer and bilayer graphene and MoS₂ as test cases. The datasets comprise DFT Hamiltonians calculated with OpenMX package [22, 23]. Datasets are sourced from Ref. [10] and are available in public repositories at Zenodo [24]. Structures of datasets are gener-

TABLE I. The mean absolute errors (MAEs) in units of meV of DFT Hamiltonian matrix elements for multiple case studies, including calculations of graphene and MoS₂ in monolayer and bilayer supercell structures. The results of DeepH [10] and DeepH-E3 [11] are listed for comparison.

	Monolayer		Bilayer	
	Graphene	MoS ₂	Graphene	MoS ₂
DeepH [10]	2.1	1.0	1.9	0.57
DeepH-E3 [11]	0.40	0.46	0.41	0.49
DeepH-2	0.12	0.21	0.17	0.19

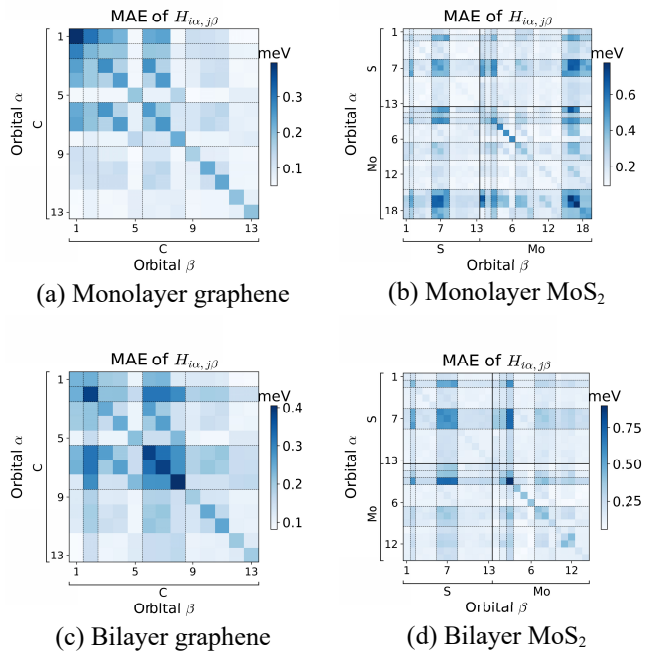


FIG. 3. Orbital-wise MAE of Hamiltonian elements of (a) monolayer graphene (b) monolayer MoS₂ (c) bilayer graphene; (d) bilayer MoS₂. MAE of all orbits reach sub-meV level.

ated with molecular dynamics or random perturbation, details are discussed in [10]. DeepH and DeepH-E3 are benchmarked and compared with DeepH-2 with the same splitting of training, validation and test sets. A summary of training results is presented in Table I, measured by mean absolute errors (MAEs) for DFT Hamiltonian matrix elements. The accuracy of DeepH-2 is more than two times higher compared with DeepH-E3 across all of these datasets, achieving an accuracy level of 0.2meV in terms of MAE. Particularly, the result for monolayer graphene reaches an unprecedented precision of 0.12meV, which is of the same order of magnitude with DFT's numerical error, demonstrating the high accuracy of DeepH-2. Furthermore, orbital-wise MAE are summarized in Fig. 3, demonstrating the model's sub-meV level accuracy for all orbitals.

Benefiting from the efficient implementation of local-coordinate-based tensor product of DeepH-2, there has been a significant increase in GPU usage rates. A

dramatic improvement in training efficiency is observed in comparison with DeepH-E3, even with a order-of-magnitude bigger amount of trainable parameters. In the case of bilayer graphene, the training time per epoch has decreased from 2.0×10^2 to 1.0×10^2 seconds. Meanwhile, the number of parameters increased from 0.07×10^7 for DeepH-E3, to 4.37×10^7 for DeepH-2, representing a 60-fold increase in the number of parameters. The high efficiency and large parameter size of DeepH-2 enable its application to more complicated datasets.

V. CONCLUSION

In summary, we introduce DeepH-2, a deep learning framework for predicting DFT Hamiltonian. The newly developed method features the realization of SO(3) equivariance based on a local-coordinate formalism, which significantly reduces the computational cost from $O(L^6)$ to $O(L^3)$, enabling the inclusion of higher-angular-momentum neural network features. Our framework also incorporates multiple advanced neural network techniques including equivariant transformer, cul-

minating in what we term an equivariant local-coordinate transformer. Through multiple case studies, we exemplified the accuracy and efficiency of DeepH-2, revealing its superiority over previous models including DeepH and DeepH-E3. Our work presents a more powerful and efficient neural network architecture for representing DFT Hamiltonians, thereby paves the way to high-accuracy electronic structure study of a broader range of large-scale materials.

VI. ACKNOWLEDGEMENT

We thank T. Bao for providing some training datasets. This work was supported by the Basic Science Center Project of NSFC (grant no. 52388201), the National Natural Science Foundation of China (grant no. 12334003), the Ministry of Science and Technology of China (grant no. 2023YFA1406400), the National Science Fund for Distinguished Young Scholars (grant no. 12025405), the Beijing Advanced Innovation Center for Future Chip (ICFC), and the Beijing Advanced Innovation Center for Materials Genome Engineering. The calculations were done on Hefei advanced computing center.

-
- [1] S. Lorenz, A. Groß, and M. Scheffler, Representing high-dimensional potential-energy surfaces for reactions at surfaces by neural networks, *Chem. Phys. Lett.* **395**, 210 (2004).
 - [2] J. Behler and M. Parrinello, Generalized neural-network representation of high-dimensional potential-energy surfaces, *Phys. Rev. Lett.* **98**, 146401 (2007).
 - [3] F. Brockherde, L. Vogt, L. Li, M. E. Tuckerman, K. Burke, and K.-R. Müller, Bypassing the kohn-sham equations with machine learning, *Nat. Commun.* **8**, 872 (2017).
 - [4] J. Gilmer, S. S. Schoenholz, P. F. Riley, O. Vinyals, and G. E. Dahl, Neural message passing for quantum chemistry, in *Proceedings of the 34th International Conference on Machine Learning (ICML)*, Vol. 70 (JMLR.org, 2017) pp. 1263–1272.
 - [5] L. Zhang, J. Han, H. Wang, R. Car, and W. E, Deep potential molecular dynamics: A scalable model with the accuracy of quantum mechanics, *Phys. Rev. Lett.* **120**, 143001 (2018).
 - [6] K. T. Schütt, H. E. Sauceda, P.-J. Kindermans, A. Tkatchenko, and K.-R. Müller, Schnet – a deep learning architecture for molecules and materials, *J. Chem. Phys.* **148**, 241722 (2018).
 - [7] T. Xie and J. C. Grossman, Crystal graph convolutional neural networks for an accurate and interpretable prediction of material properties, *Phys. Rev. Lett.* **120**, 145301 (2018).
 - [8] S. Batzner, A. Musaelian, L. Sun, M. Geiger, J. P. Mailoa, M. Kornbluth, N. Molinari, T. E. Smidt, and B. Kozinsky, E(3)-equivariant graph neural networks for data-efficient and accurate interatomic potentials, *Nat. Commun.* **13**, 2453 (2022).
 - [9] A. Musaelian, S. Batzner, A. Johansson, L. Sun, C. J. Owen, M. Kornbluth, and B. Kozinsky, Learning local equivariant representations for large-scale atomistic dynamics, *Nat. Commun.* **14**, 579 (2023).
 - [10] H. Li, Z. Wang, N. Zou, M. Ye, R. Xu, X. Gong, W. Duan, and Y. Xu, Deep-learning density functional theory hamiltonian for efficient ab initio electronic-structure calculation, *Nat. Comput. Sci.* **2**, 367–377 (2022).
 - [11] X. Gong, H. Li, N. Zou, R. Xu, W. Duan, and Y. Xu, General framework for E(3)-equivariant neural network representation of density functional theory hamiltonian, *Nat. Commun.* **14**, 10.1038/s41467-023-38468-8 (2023).
 - [12] H. Li, Z. Tang, X. Gong, N. Zou, W. Duan, and Y. Xu, Deep-learning electronic-structure calculation of magnetic superstructures, *Nat. Comput. Sci.* **3**, 321–327 (2023).
 - [13] H. Li and Y. Xu, Improving the efficiency of ab initio electronic-structure calculations by deep learning, *Nat. Comput. Sci.* **2**, 418 (2022).
 - [14] H. Li and Y. Xu, A deep-learning method for studying magnetic superstructures, *Nat. Comput. Sci.* **3**, 287 (2023).
 - [15] Z. Tang, H. Li, P. Lin, X. Gong, G. Jin, L. He, H. Jiang, X. Ren, W. Duan, and Y. Xu, Efficient hybrid density functional calculation by deep learning, *arXiv preprint arXiv:2302.08221* (2023).
 - [16] E. Prodan and W. Kohn, Nearsightedness of electronic matter, *Proc. Natl. Acad. Sci. USA* **102**, 11635 (2005).
 - [17] S. Passaro and C. L. Zitnick, Reducing SO(3) convolutions to SO(2) for efficient equivariant GNNs, *arXiv preprint arXiv:2302.03655* (2023).

- [18] Y.-L. Liao, B. Wood, A. Das, and T. Smidt, EquiformerV2: Improved equivariant transformer for scaling to higher-degree representations, [arXiv preprint arXiv:2306.12059](#) (2023).
- [19] R. M. Martin, *Electronic structure: basic theory and practical methods* (Cambridge university press, 2020).
- [20] W. Kohn, Density functional and density matrix method scaling linearly with the number of atoms, *Phys. Rev. Lett.* **76**, 3168 (1996).
- [21] M. Geiger and T. Smidt, e3nn: Euclidean neural networks, [arXiv preprint arXiv:2207.09453](#) (2022).
- [22] T. Ozaki, Variationally optimized atomic orbitals for large-scale electronic structures, *Phys. Rev. B* **67**, 155108 (2003).
- [23] T. Ozaki and H. Kino, Numerical atomic basis orbitals from H to Kr, *Phys. Rev. B* **69**, 195113 (2004).
- [24] X. Gong, H. Li, N. Zou, R. Xu, W. Duan, and Y. Xu, Dataset1 for “General framework for E(3)-equivariant neural network representation of density functional theory Hamiltonian”, [10.5281/zenodo.7553640](#) (2023).
- [25] K. T. Schütt, M. Gastegger, A. Tkatchenko, K.-R. Müller, and R. J. Maurer, Unifying machine learning and quantum chemistry with a deep neural network for molecular wavefunctions, *Nat. Commun.* **10**, 5024 (2019).
- [26] A. Paszke, S. Gross, F. Massa, A. Lerer, J. Bradbury, G. Chanan, T. Killeen, Z. Lin, N. Gimeshain, L. Antiga, A. Desmaison, A. Kopf, E. Yang, Z. DeVito, M. Raison, A. Tejani, S. Chilamkurthy, B. Steiner, L. Fang, J. Bai, and S. Chintala, Pytorch: An imperative style, high-performance deep learning library, in *Advances in Neural Information Processing Systems 32*, edited by H. Wallach, H. Larochelle, A. Beygelzimer, F. d'Alché-Buc, E. Fox, and R. Garnett (Curran Associates, Inc., 2019) pp. 8024–8035.
- [27] M. Geiger, T. Smidt, A. M., B. K. Miller, W. Boomsma, B. Dice, K. Lapchevskyi, M. Weiler, M. Tyszkiewicz, S. Batzner, M. Uhrin, J. Frellsen, N. Jung, S. Sanborn, J. Rackers, and M. Bailey, [e3nn/e3nn: 2021-08-27](#) (2021).